Mathematical modeling and analysis of hot carrier solar cells

Author:
BENJAMIN VAN DIJK

Supervisor:
PETER SAMUELSSON
Co-supervisor:
ADAM BURKE

LUNDS UNIVERSITET

DEPARTMENT OF PHYSICS
DIVISION OF MATHEMATICAL PHYSICS
EXAMINATION: 11TH OF MAY 2023, DURATION: 2 MONTHS
TYPE OF DIPLOMA WORK: BACHELOR THESIS

Contents

Abstract

This thesis focuses on the analysis of a mathematical model of a nanowire based hot carrier solar cell. The relevance of the topic comes from the energy crisis society is facing today. Firstly, we discuss the basic principle of hot carrier solar cells and discuss several energy loss factors. Then we set up the system and discuss the relevant approximations. Moreover analytical expressions of the carrier and heat current are derived in order to determine the maximum power, efficiency and Fill factor of the solar cell. Different parameters like the potential barrier height within the solar cell are investigated such that their trends in the overall performance can be determined. The model represents a very ideal case and does not take many loss mechanisms into consideration. Therefore the thesis has many future research possibilities so it can be applied in the laboratory.

Acknowledgements

Firstly I would like to thank my main supervisor Peter for the great mentor ship in this period. I have received the impression that his main priority along the entire project was to make the experience as pedagogical as possible for me. Whenever help was needed he made time from his busy schedule which I am very grateful for. Moreover, he set many meetings with additional people within related fields to my topic such that I could get a broader perspective. Not only did he help me with the underlying physics but with the entire process as well. Since I had never written a thesis before it was extremely helpful to receive guidance throughout the semester. Furthermore, I want thank the other bachelor, master, PHD and postdoc students within Peter's working group for many interesting input, physics presentations and pleasant group meetings. Finally, I want to thank my co-supervisor Adam Burke for giving interesting experimental knowledge related to my thesis.

1 Introduction

One of the main challenges society is facing today is for mankind to find sustainable energy sources. Solar cells are a perfect candidate for this since no green house gasses are emitted in the energy production. Moreover, the energy solar radiation gives to the earth in an hour can produce the entire world with sufficient energy for a year [1] However, the efficiency of the majority of current solar cells produced in the industry are still under 20% [2]. For this reason scientists and engineers have been heavily conducting research finding methods to optimize the efficiency of solar cells.

Typically, silicon based solar cells are produced on a large scale due to the accessibility in nature and high abundance of the material. Nonetheless, currently there are more efficient photovoltaic devices available. An example of these are solar cells based on type III-V semiconductor materials such as gallium arsenide and indium phosphide. The disadvantage of III-V based solar cells is that the materials are expensive which makes it hard to apply to industry[3][4]. An innovating solution for this is the use of nano scaled rod-like structures with a high length/diameter ratio, also known as nanowires[5]. Due to their dimensional properties 90% less of the expensive III/V materials has to be used with respect to the solar cells manufactured as thin film[3].For this reason nanowires are promising for the future development of solar cells.

This thesis will focus on a mathematical model which simulates the phenomena happening in a nanowire based hot carrier solar cell. To do this we firstly consider the basic concept of a solar cell and discuss different energy loss mechanisms which can occur. Then we will make the model in the ideal case to extract the power production and efficiency.

2 Theory

2.1 Principle of solar cell and loss mechanisms

In order to manufacture a hot carrier solar cell one creates material with different semiconductors. When various semiconducting materials are combined, it results in different potential barriers in both the valence and conduction band.[6] Creating this structure in a nanowire will give the characteristics in the conduction and valence band as shown in figure 1.

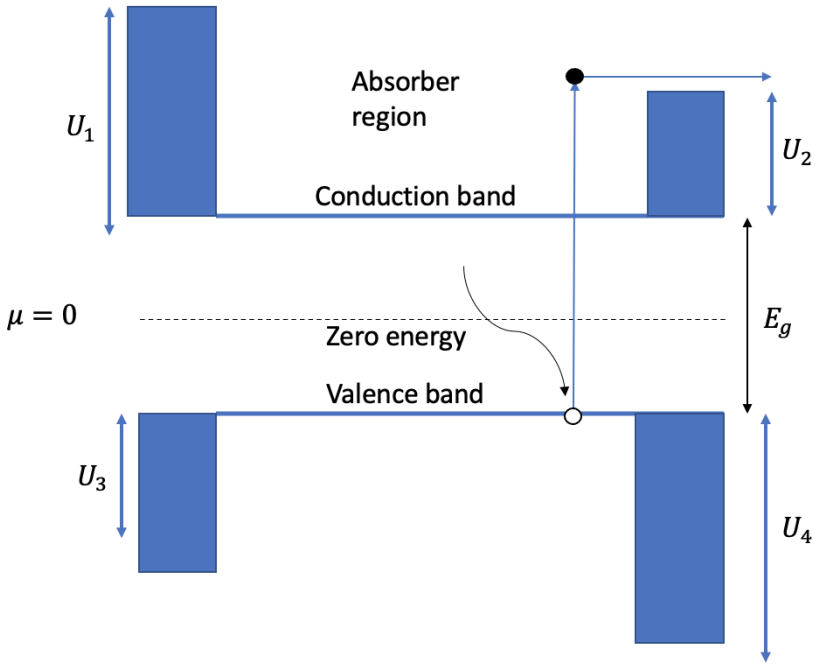

Figure 1: Energy diagram of a hot carrier solar cell. It can be seen that 4 different potential barriers arise. The curly arrow represents light interacting with electrons in the valence band creating an electron hole pair. If the absolute energy of the electron is higher than $E_g + U_2$ it can go over the potential barrier U_2 and create an electrical current. In order for charge to be conserved the chemical potential has been fixed at $E_g/2$ where the zero energy axis is defined.

In figure 1 it can be seen that four different potential barriers are created. When a photon comes in with energy larger than $E_g + U_2$, it can excite an electron which can go over the potential barrier U_2 and create an electrical current. However, the efficiency of a solar cell is influenced by many factors. Often the following four are considered [7]:

1. **Carnot energy loss**: The Carnot efficiency defines the fundamentally highest efficiency which can be achieved for a power conversion process which behaves like a heat engine [8]. It is fixed by the temperature of the heat source and the power converter. In our case we model the heat source to be a piece of metal connected to the

solar cell absorbing solar photons. If the metal slap would be in thermal equilibrium with the sun, the temperature of the heat source would be at the temperature of the sun $T_S = 5772$ K. Moreover, the temperature of the solar cell itself is assumed to be at room temperature $T_r = 300$ K. This implies that the maximum Carnot efficiency will be $(T_S - T_r)/T_S$= 95%.

2. **Band gap**: Here we consider the fact that only photons with energy larger than the band gap of the material will be excited to the conduction band. This means that photons with an energy smaller than the band gap E_g will not contribute in the generation of electrical current.

3. **Recombination**: Once a photon has more energy than the band gap E_g it creates a hole in the valence band and an electron in the conduction band. However, it is possible for the electrons to recombine with their respective hole instead of contributing to the power production. Along this process radiation will be emitted.

4. **Carrier relaxation**: Once a photon is excited with energy higher than the potential barrier of the solar cell, it can either go over the barrier to produce electricity or it can loose parts of its energy through various processes. The carrier can thermalize with other carriers through inelastic collisions or interact with lattice vibrations and convert its energy in the form of heat. An electron of this sort is defined as a hot carrier [5].

To keep calculations simple we will only take the band gap loss and the Carnot efficiency into consideration for the model discussed in the thesis. However more of the above effects can in principle be added to give a more realistic result.

3 The model

This section will describe the model used to simulate the behaviour of the solar cell. A visualisation of the model is found in figure 2. Firstly we assume the potential barriers to be asymmetric in the conduction and valence band. Here the left side and right side represent the contact for the holes and electrons respectively. At the left side of the conduction band the potential barrier U_h is set infinitely high and the potential barrier on the right side is set to the fixed value U_e. Between the four barriers is were the absorber region is located.

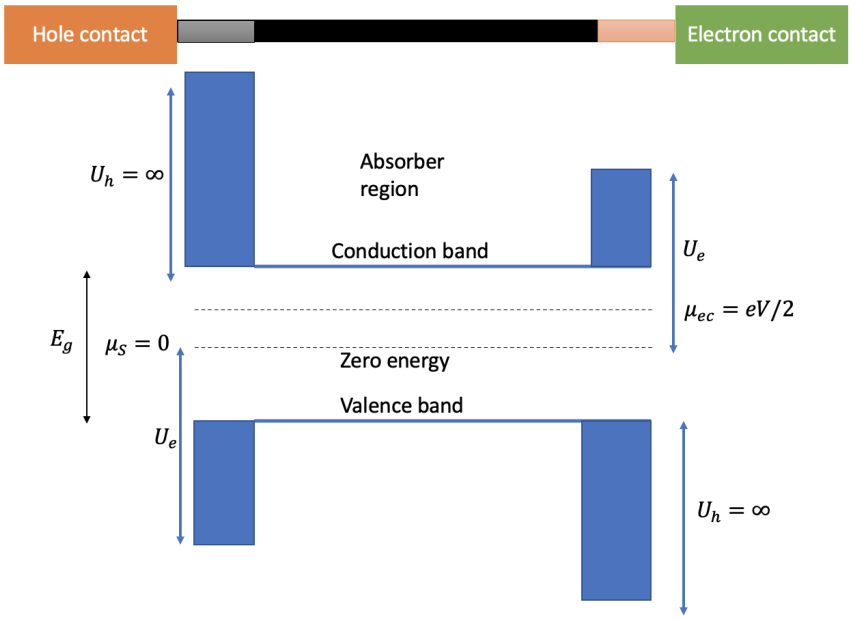

Figure 2: Illustration of the model. Compared to figure 1 $U_1 = U_4 = U_h = \infty$ and $U_2 = U_3 = U_e$. The zero energy axis is set to be in the middle of the valence and conduction band. Moreover, the chemical potential of the sun reservoir and electron collector is set at $\mu_S = 0$ and $\mu_{ec} = eV/2$ respectively. The left hand side of the model has a direct hole contact and the right side represents the electron contact. Finally the grey area represents a material composition such that the potential barriers U_e and U_h arise, the black region for the absorber region and the red zone the barriers U_e and U_h in the opposite manner with respect to the grey zone.

For the model we only distinguish electrons and holes from having the opposite sign in charge and neglect other differences such as the difference in effective mass. Finally, the zero energy is set at half the energy of the band gap E_g.

In order to describe the effects occurring in a photovoltaic device we model the absorber to be coupled to two reservoirs:

1. **Electron collector**: This probe models the contact which extracts the electrons from the absorber and generates a current. Its temperature is assumed to be equal to room

temperature $T_{ec} = 300K$. The chemical potential will be equal to the bias applied. Due to the symmetry of the system this would simply be $\mu_{ec=} + eV/2$ and with corresponding Fermi function $f_{ec}(E)$. The chemical potential on the left side of the system will have the same behaviour but with opposite sign.

2. **The sun**: This reservoir serves for the incoming light of the sun which is heating up the system and exciting electrons. It is represented with a Fermi-Dirac distribution $f_S(E)$ and corresponding temperature $T_S = T_{ec} + \Delta T$. Here ΔT represents the extra temperature the sun reservoir has with respect to the electron collector. Finally, the chemical potential is set to $\mu_S = 0$. In real life this reservoir is a photo-antenna place on the nanowire to locally heat up the system.

Here the Fermi functions $f_i(E)$ are of the form

$$f_i(E) = \frac{1}{1 + e^{\beta_i(E-\mu_i)}}, \tag{1}$$

where $\beta_i = 1/K_B T_i$. The absorber function $f_A(E)$ is a superposition of the two Fermi functions. Its time derivative can be represented as [9]

$$\frac{\partial f_A(E,t)}{\partial t} = \Gamma_S(f_S(E,t) - f_A(E,t)) + \Theta(E - U_e)\Gamma_{ec}(f_{ec}(E,t) - f_A(E,t)), \tag{2}$$

where Γ_i denotes the rate of the probe i and $\Theta(E - U_e)$ the heavy side step function which is 0 if $E < U_e$ and 1 for $E \geq U_e$. The step function arises from the assumption that electrons can only go over the potential barrier if their energy is greater or equal than U_e. Equation (2) is a continuity equation of the system and is a mathematical formulation that all charge carriers are conserved. For the further analysis we assume the system is in a steady state, implying that the time derivative of the absorber is equal to zero. This will result the solution of the differential equation to be equal to

$$f_A(E) = \frac{\Gamma_S f_S(E) + \Theta(E - U_e)\Gamma_{ec} f_{ec}(E)}{\Gamma_S + \Theta(E - U_e)\Gamma_{ec}}. \tag{3}$$

3.1 Charge and energy currents

Using scatter theory, the carrier current I_n^N and energy current I_n^E flowing from reservoir m to n will be defined as [9]

$$I_n^N = \Gamma_n \int_{E_g/2}^{\infty} [f_n(E) - f_m(E)]\, dE, \tag{4}$$

$$I_n^E = \Gamma_n \int_{E_g/2}^{\infty} (E - \mu_n)\, [f_n(E) - f_m(E)]\, dE. \tag{5}$$

The integration limits are chosen such that we will only integrate over the electrons located with energy states in the conduction band. In this model only two probes are coupled with the absorber. Thus, only the current from the sun reservoir to the absorber I_S

and the current from the electron collector to the absorber I_{ec} have to be calculated. For the carrier current one obtains the expressions

$$I_S^N = \Gamma_S \int_{E_g/2}^{\infty} [f_S(E) - f_A(E)]\, dE, \tag{6}$$

$$I_{ec}^N = \Gamma_{ec} \int_{U_e}^{\infty} [f_{ec}(E) - f_A(E)]\, dE. \tag{7}$$

When the integrals are solved it turns out that $I_s^N = -I_{ec}^N$. This is exactly what we would expect since the total amount of carriers entering and leaving the absorber has to be conserved. The solution for the electron collector's current is given by

$$I_{ec}^N = \frac{\Gamma_S \Gamma_{ec}}{\beta_S \beta_{ec}(\Gamma_{ec} + \Gamma_S)} \cdot \Big(\beta_S \log\Big(e^{\beta_{ec}(U_e - \mu_{ec})} + 1\Big) \\ - \beta_{ec} \log\Big(e^{\beta_S(U_e - \mu_S)} + 1\Big) + \beta_S \beta_{ec}(\mu_{ec} - \mu_S)\Big). \tag{8}$$

The corresponding energy currents are denoted as:

$$I_S^E = \Gamma_S \int_{E_g/2}^{\infty} (E - \mu_S)\, [f_S(E) - f_A(E)]\, dE, \tag{9}$$

$$I_{ec}^E = \Gamma_{ec} \int_{U_e}^{\infty} (E - \mu_{ec})\, [f_{ec}(E) - f_A(E)]\, dE. \tag{10}$$

Similarly as for the charge currents it turns out that $I_S^E = -I_{ec}^E$. Therefore we will only write down the solution for the solar current:

$$I_S^E = \frac{\Gamma_{ec}\Gamma_S}{\beta_{ec}^2 \beta_S^2 (\Gamma_{ec} + \Gamma_S)} \Big[\beta_{ec}^2 \Big(Li_2(-e^{-\beta_S(U_e - \mu_s)}) + \beta_S(U_e - \mu_S) \log\Big(e^{-\beta_S(U_e - \mu_S)} + 1\Big)\Big) \\ - \beta_S^2 \Big(Li_2(-e^{-\beta_{ec}(U_e - \mu_{ec})}) + \beta_{ec}(U_e - \mu_{ec}) \log\Big(e^{-\beta_{ec}(U_e - \mu_{ec})}\Big)\Big) \\ - \mu_{ec}\beta_{ec}\beta_S^2 \cdot \Big(\log\Big(e^{\beta_{ec}(U_e - \mu_{ec})} + 1\Big) - \beta_{ec}(U_e - \mu_{ec})\Big)\Big] \tag{11}$$

where $Li_2(x)$ is the Spence function defined as [10]

$$Li_2(x) = -\int_0^x \frac{\log(1-t)}{t} dt,\ \forall x \in \mathbb{C}. \tag{12}$$

3.2 Power production and performance of solar cell

In order to find the performance of the solar cell we have to define the power generated by the device. In this model power is produced when the carrier current I_{ec}^N moves against the chemical potential μ_{ec} [9]. For this reason, we denote the total net power to be

$$P = 2 \cdot I_{ec}^N \cdot \mu_{ec}/2 = I_{ec}^N eV. \tag{13}$$

The factor of two arises from the electron-hole symmetry. For each electron flowing to the right side of the conduction band in figure 2, a respective hole will travel to the left side of the valence band. Hence, the power produced by the electrons can be multiplied by 2 in order to obtain the total power. Figure 3 visualizes how the power is generated. Due to a larger temperature T_S the sun's Fermi function is extended over the potential barrier U_e. Therefore, electrons from the sun reservoir are able to move towards the electron collector. Finally, we define the efficiency η to be the fraction of the power for a given T_S and V and the corresponding heat current of the sun I_S^E

$$\eta = \frac{P}{I_S^E}. \tag{14}$$

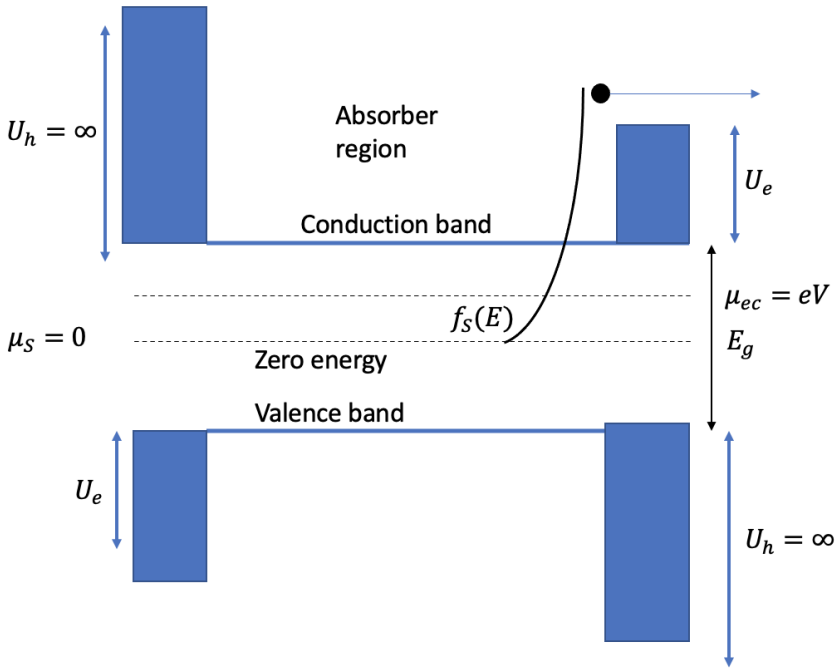

Figure 3: The system with a high temperature T_S. Here the Fermi function $f_S(E)$ is extended such that some of its electron's energy is higher than the potential barrier. This allows it to move to the electron collector and create a net charge current.

Another way to quantify the performance of the solar cell than efficiency, is through the Fill factor. It is defined with the equation

$$FF = \frac{P_{max}}{I_{sc} \cdot V_{oc}}, \tag{15}$$

where I_{sc} is the short circuit current, V_{oc} the open circuit voltage and P_{max} the maximum produced power [11]. The short circuit current represents the current at zero voltage.

Furthermore the open circuit voltage is defined to be the voltage where no current is flowing [12]. Figure shows an $I - V$ curve with these quantities marked down. A Fill factor of 1 represents the highest theoretical power that can be extracted from the I-V curve and means that the I-V curve would look like the black dotted line shown in figure 4. However in reality this has never been achieved experimentally. The higher the Fill factor, the higher the maximum power of the I-V curve becomes [13].

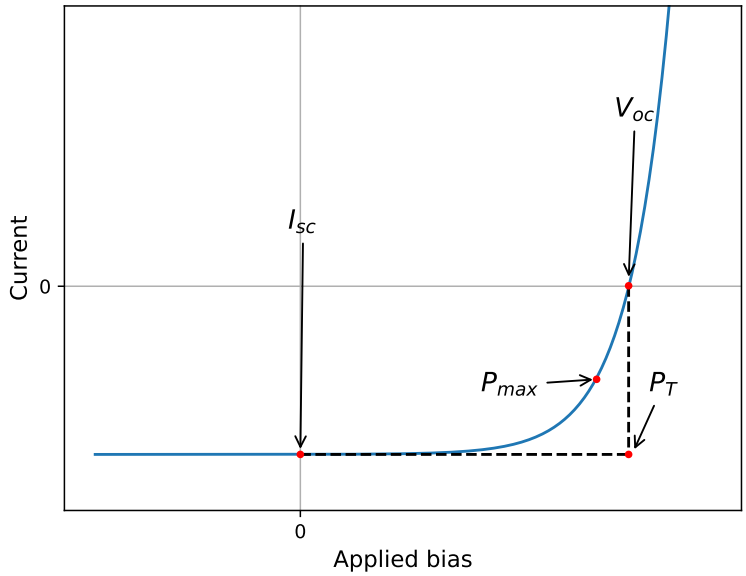

Figure 4: I-V curve showing the quantities of the Fill factor. Here I_{sc} represents the short circuit current and V_{oc} the open circuit voltage. P_{max} and P_T represent the location where the maximum power of the I-V curve and the theoretical maximum power is located respectively.

3.3 Dimensionless expressions

For the purpose of extracting results from the equations introduced in section 3.1, we will rewrite them in a dimensionless form. Firstly, we introduce the following dimensionless parameters

$$\epsilon \equiv \beta_{ec} U_e, \tag{16}$$

$$\gamma_S \equiv \frac{1}{1 + \frac{\Delta T}{T_{ec}}}, \tag{17}$$

$$\chi \equiv \beta_{ec} \mu_{ec}, \tag{18}$$

Now by dividing the carrier currents by $I_0 = \frac{\Gamma_S \Gamma_{ec}}{(\Gamma_S + \Gamma_{ec})\beta_{ec}}$ and substituting the parameters by the dimensionless quantities defined in equations (16), (17) and (18) we obtain the

following for the carrier current of the electron collector.

$$\tau_{ec}^{N} = \frac{I_{ec}^{N}}{I_0} = \log\left(e^{\epsilon-\chi}+1\right) - \frac{1}{\gamma_S}\log(e^{\gamma_S\cdot\epsilon}+1) + \chi. \tag{19}$$

$$\tag{20}$$

Similarly for the energy current of the sun reservoir we obtain

$$\begin{aligned}&\tau_S^E = \frac{I_S^E}{I_0'} = \\ &\frac{1}{\gamma_S^2}\cdot\left(Li_2(-e^{-\gamma_S\epsilon}) + \gamma_S\epsilon\log\left(e^{-\gamma_S\epsilon}+1\right)\right) - \left(Li_2(-e^{\chi-\epsilon}) + (\epsilon-\chi)\log\left(e^{-\epsilon\gamma_S}+1\right)\right) \\ &-\chi\left(\log\left(e^{\epsilon-\chi}+1\right) - (\epsilon-\chi)\right)\end{aligned} \tag{21}$$

where $I_0' = \frac{\Gamma_{ec}\Gamma_S}{\beta_{ec}^2(\Gamma_{ec}+\Gamma_S)}$. To continue, we define the equivalent to dimensionless power to be:

$$\rho \equiv \tau_{ec}\cdot\chi. \tag{22}$$

The derivation for the substitutions can be found in the appendix.

4 Results and discussion

4.1 Charge currents

In figure 5a and 5b the electron collector's carrier current is plotted with varying the parameters $\frac{\Delta T}{T_{ec}}$ and ϵ respectively.

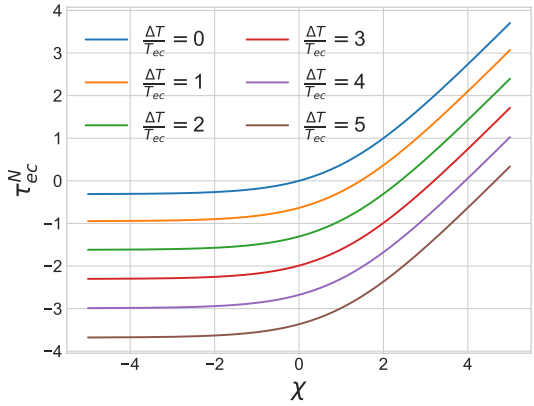

(a) The carrier current of the electron collector plotted against the bias applied to the system. Here the current is plotted for different values of $\frac{\Delta T}{T_{ec}}$ and ϵ has been fixed to 1

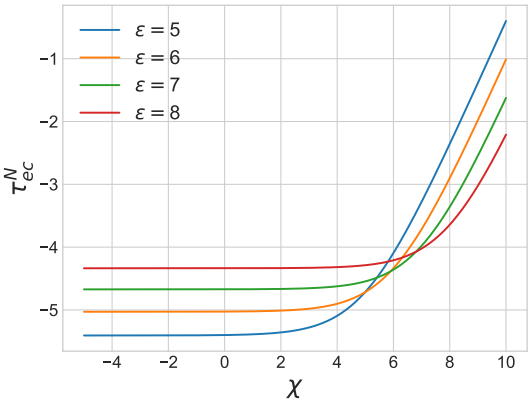

(b) Here the carrier current of the electron collector is plotted vs the applied bias. Multiple values for the potential barrier heights ϵ are shown in the figure and $\frac{\Delta T}{T_{ec}}$ has been set to 10

Figure 5: The carrier currents of the electron collector plotted against the applied voltage. Parameters $\frac{\Delta T}{T_{ec}}$ and ϵ are altered for figure 5a and 5b respectively.

Remark that a negative current in figures 5a and 5b implies that current is flowing **from the absorber to the electron collector** due to its definition in equation 7. In figure 5a we can observe that $\tau_{ec}^N = 0$ for $\chi = 0$ when $\frac{\Delta T}{T_{ec}} = 0$. This is due to the fact that in this case there is no temperature difference between the sun reservoir and the electron collector. Moreover since $\chi = 0$ in this instant, their Fermi functions will be identical. Consequently, no current can flow either to the absorber or the electron collector. As illustrated in figure 3 the Fermi function of the sun gets more extended for higher values of $\frac{\Delta T}{T_{ec}}$. Because of this, more electrons in the electron distribution of the sun get an energy higher than the potential barrier U_e which will cause a net charge current towards the electron collector for 0 applied bias. This is why when the parameter $\frac{\Delta T}{T_{ec}}$ increases in figure 5a, the offset of the current goes to more negative values. Because μ_{ec} is proportional to the voltage, the Fermi function of the electron collector will reach higher energy levels as the voltage applied to the system increases. Therefore, the τ_{ec}^N grows as the applied bias becomes larger.

From figure 5b it can be seen that an increasing value of ϵ moves up the current to a higher offset. Hence, less charge carriers are moving towards the electron collector with a higher potential barrier. This comes from the fact that the charge carriers are required

to have a higher energy to surpass a larger potential barrier U_e. Another observation is that for a bigger value of ϵ the current starts to increase at a larger value of χ with respect to a smaller ϵ. The reason for this is that the electron distribution in the electron collector needs to have a higher energy to overcome a larger potential barrier U_e. Thus, the chemical potential of the electron collector μ_{ec} has to become larger for an increase of current to occur.

4.2 Net power and heat current of the solar cell

The resulting net power produced by the device can be calculated through equation 22. This has been done in figures 6a and 6b for varying values of $\frac{\Delta T}{T_{ec}}$ and ϵ respectively. It can be seen in 6a that the power increases as the temperature of the sun reservoir grows. This is simply because a higher $\frac{\Delta T}{T_{ec}}$ give more current towards the electron collector and needs more applied bias to give a positive τ_{ec}^N.

Figure 6b shows that higher values of ϵ for a fixed $\frac{\Delta T}{T_{ec}}$ result in a higher maximum power than smaller values of ϵ. This seems counter intuitive since the results in figure 5b showed that less charge carriers move to the electron collector for higher values of ϵ. Nonetheless, more bias has to be applied in order for τ_{ec}^N to increase. The power is proportional to both current and voltage and since the bias difference is substantially higher than the current difference for $\epsilon < 8$, more maximum power is achieved for higher values of ϵ. Both figure 6a and 6b show that for a fixed ϵ and $\frac{\Delta T}{T_{ec}}$ the power reaches a maximum ρ_{max} at a bias χ_{max}. Figure 7 shows this maximum power plotted against $\frac{\Delta T}{T_{ec}}$ for multiple values of ϵ. The same is done for the heat current of the sun reservoir τ_S^E in figure 8.

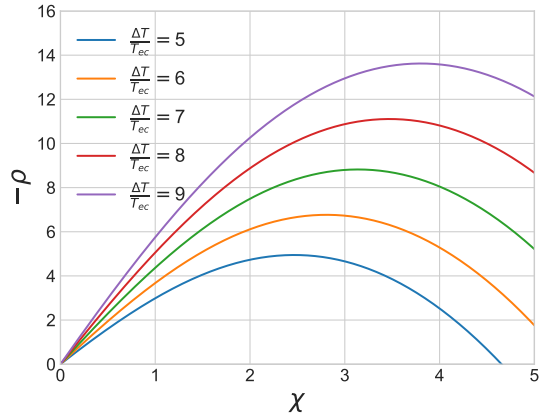

(a) Produced power of the solar cell plotted against the applied bias for different values of $\frac{\Delta T}{T_{ec}}$. In this case $\epsilon = 1$ for all curves.

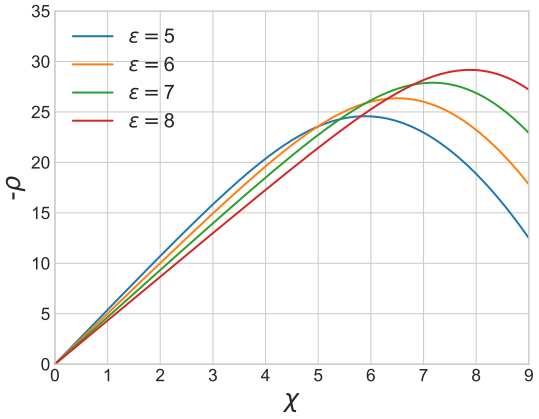

(b) The net power of the solar cell plotted against the applied bias. The parameter ϵ has been varied and $\frac{\Delta T}{T_{ec}}$=10 for all the graphs.

Figure 6: The net power produced by the device plotted against the bias applied to the system. Figures 6a and 6b vary the parameters $\frac{\Delta T}{T_{ec}}$ and ϵ respectively. Remark that negative power implies that a net energy flow is traveling towards the electron contact. Therefore, for convenience the negative power has been labeled on the y-axis.

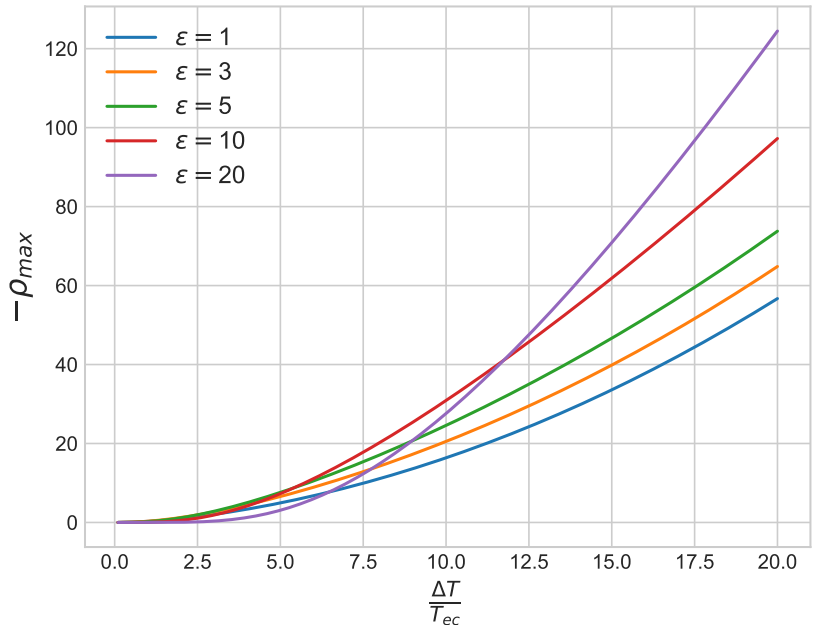

Figure 7: Maximum power plotted against $\frac{\Delta T}{T_{ec}}$ for different ϵ. The respective χ_{max} has been chosen for each $\frac{\Delta T}{T_{ec}}$. Four different values of ϵ have been chosen for the curve to show the trend.

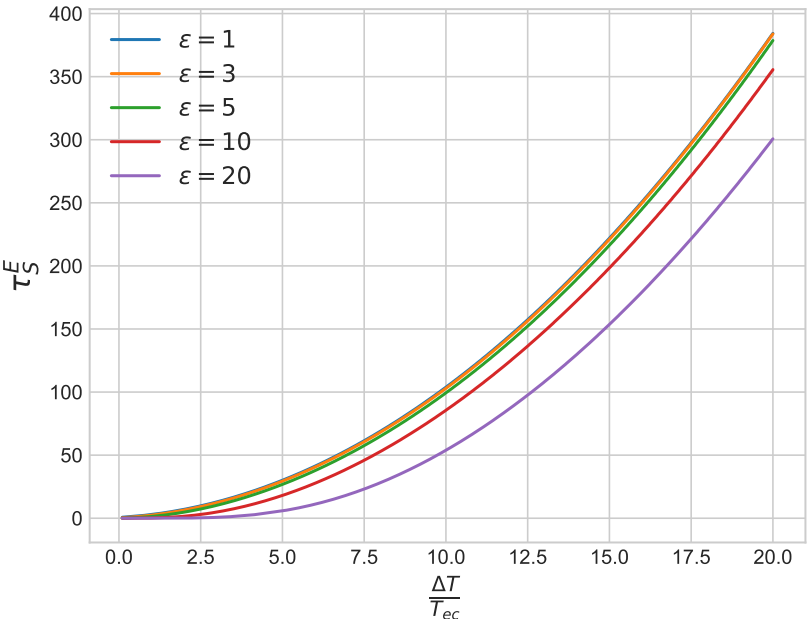

Figure 8: The heat current of the sun reservoir plotted against different values of $\frac{\Delta T}{T_{ec}}$. The same values for χ_{max} have been chosen as the ones in figure 7. Note that a positive value of τ_S^E implies that the current is going from the sun reservoir towards the absorber region.

Figure 7 shows that the maximum power is strictly increasing as $\frac{\Delta T}{T_{ec}}$ grows. The reason why the maximum power is not converging to a constant is due to the Fermi function of the sun. In equation 1 we can note that when $\frac{\Delta T}{T_{ec}} \longrightarrow \infty \implies \beta_S \longrightarrow 0$. This causes the Fermi function of the sun to reach a constant of $\frac{1}{2}$ for all energy values. Thus, the integral defined in equation (9) will diverge when $\frac{\Delta T}{T_{ec}} \longrightarrow \infty$. Nonetheless, these temperatures can never be achieved in reality since the nanowire itself would melt.

Furthermore, a similar trend as found in 6b can be seen in figure 7. For larger values of $\frac{\Delta T}{T_{ec}}$ a higher ϵ results in more power with respect to a smaller ϵ. However, from figure 7 it can be seen that when $\epsilon \geq 10$ the power becomes lower for smaller $\frac{\Delta T}{T_{ec}}$ compared to lower magnitudes of ϵ. For example $-\rho_{max}$ at $\epsilon = 5$ is larger than ρ_{max} at $\epsilon = 10$ up until $\frac{\Delta T}{T_{ec}} = 8.8$. In reality this means that the metal probe connected to the nanowire representing the sun reservoir has a temperature around 3000 K. In order to produce a nanowire with this barrier height the materials used to fabricate it would have to withstand this amount of heat and cannot melt.

The heat current of the sun decreases for larger values of ϵ. For a higher potential barrier U_e only high energy electrons can travel to the electron collector. Therefore the heat current decreases as ϵ increases. On the contrary, the heat current still stays substantially larger than the net power.

4.3 Efficiency and performance of the solar cell

In order to investigate the performance of the solar cell we will both look at its efficiency and Fill factor at maximum power. The efficiency shown in figure 9a was computed with equation (14) and the Fill factor plotted in figure 9b was determined with equation (3.2).

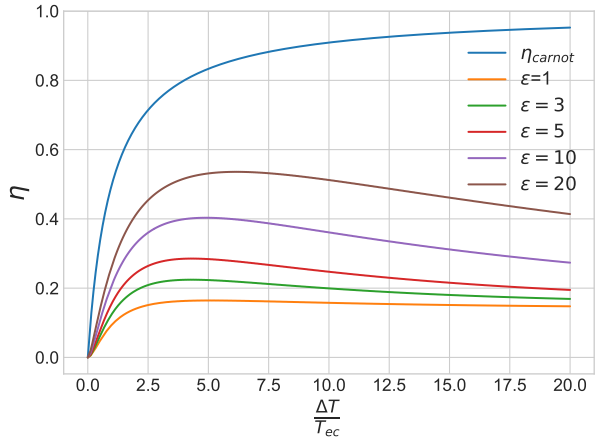

(a) The efficiency of the solar cell at maximum power plotted against $\frac{\Delta T}{T_{ec}}$ for different values of ϵ. The efficiency has been computed by dividing each $-\rho_{max}$ in figure 7 with the respective τ_S^E shown in figure 8. Finally, the blue curve represents Carnot efficiency which can fundamentally not be exceeded.

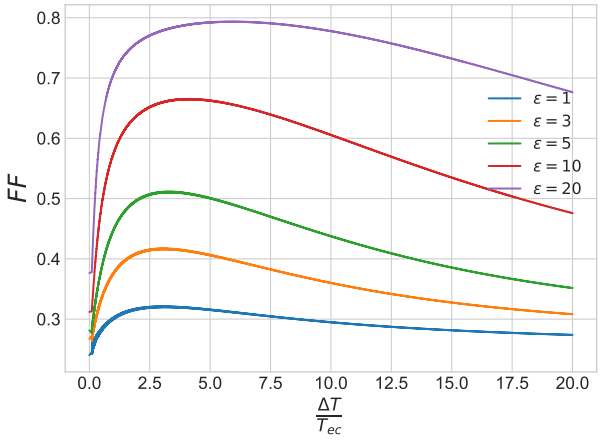

(b) Fill factor plotted against $\frac{\Delta T_{ec}}{T_S}$ when maximum power is produced. The parameters used to produce this plot all come from figure 7 and 8.

Figure 9: The efficiency and Fill factor plotted when the device is producing its maximum power.

Firstly, figure 9a gives that the efficiency reaches a clear maximum at a given temperature but under η_{carnot}. All these maximums are getting higher and slightly shifted to higher temperatures of the sun reservoir as ϵ increases. The same trend is observed for the Fill factor in figure 9b.

5 Outlook

For the model used in this thesis it can be seen that a non-negligible amount of power is produced by the solar cell as the temperature of the sun reservoir grows. Furthermore, both the efficiency and Fill factor of the maximum power increases for a higher potential barrier height. In order to produce the solar cell in reality an optimum has to be found between the barrier height U_e and the temperature of the sun reservoir T_S. For higher T_S the net power increases but efficiency decreases. Moreover the device can produce more net power at higher values of T_s for a large potential barrier but a higher temperature will give less efficiency and Fill factor. In addition, one has to make sure that the nanowire itself can withstand the temperature required for a large power production without melting. Therefore a possible continuation of the thesis is to find an optimum of the named parameters and find materials optimal for the conditions.

In the model we only take two loss mechanism discussed in section 2.1 into consideration. One can however incorporate more of these loss factors to obtain a more realistic result. A suggestion on how to do this is to give every depletion process their own reservoir coupled to the absorber. Similar methods as used in this thesis can then be used to extract the carrier and heat current. The only difference would be that the absorber function defined in equation (2) becomes longer which makes the carrier and heat current integrals harder to handle. When more probes are coupled to the absorber, one can use experimental data for time scales of when events such as recombination and phonon interaction happen to give a value to the rate constant Γ_i. In this thesis the rate constant Γ_i has not been considered in the results since only two reservoirs were connected to the absorber. However when the system contains over 4 reservoirs, Γ_i becomes more relevant for realistic results.

In conclusion, the findings of the trends in the thesis are promising. Nonetheless before the model can be created in the laboratory, a significant amount of additional research needs to be conducted.

References

[1] Xiaodong Wang and service) SpringerLink (Online. *High-Efficiency Solar Cells. [Elektronisk resurs] Physics, Materials, and Devices.* Springer Series in Materials Science: 190. Springer International Publishing, 2014. ISBN: 9783319019871. URL: https://ludwig.lub.lu.se/login?url=https://search.ebscohost.com/login.aspx?direct=true&AuthType=ip,uid&db=cat07147a&AN=lub.6176576&site=eds-live&scope=site.

[2] Martin Green et al. "Solar cell efficiency tables (version 57)". In: *Progress in Photovoltaics: Research and Applications* 29.1 (2021), pp. 3–15. DOI: https://doi.org/10.1002/pip.3371.

[3] Lukas Hrachowina. *Growth and Characterization of Tandem-Junction Photovoltaic Nanowires.* Division of Solid State Physics, Department of Physics, Faculty of Engineering, Lund University, 2022. ISBN: 9789180392099. URL: https://ludwig.lub.lu.se/login?url=https://search.ebscohost.com/login.aspx?direct=true&AuthType=ip,uid&db=cat07147a&AN=lub.7120329&site=eds-live&scope=site.

[4] Pradip Kumar Chakraborty, Bholanath Mondal, and Biswadeep Chaudhuri. "Laser-induced modulation of optical band-gap parameters in the III–V-type semiconductors from the density-of-state (DOS) calculations." In: *Pramana - Journal of Physics* 92.6 (2019). ISSN: 09737111. URL: https://ludwig.lub.lu.se/login?url=https://search.ebscohost.com/login.aspx?direct=true&AuthType=ip,uid&db=edselc&AN=edselc.2-52.0-85063634906&site=eds-live&scope=site.

[5] Jonatan Fast. *Hot-carrier extraction in nanowires.* [Division of Solid State Physics], Department of Physics, Faculty of Engineering, Lund University, 2022. ISBN: 9789180395014. URL: https://ludwig.lub.lu.se/login?url=https://search.ebscohost.com/login.aspx?direct=true&AuthType=ip,uid&db=cat07147a&AN=lub.7286376&site=eds-live&scope=site.

[6] Philip Hofmann. *Solid state physics : an introduction. [Elektronisk resurs] an introduction.* Wiley-VCH, 2015. ISBN: 9783527412822. URL: https://ludwig.lub.lu.se/login?url=https://search.ebscohost.com/login.aspx?direct=true&AuthType=ip,uid&db=cat07147a&AN=lub.5581319&site=eds-live&scope=site.

[7] Louise C. Hirst and Nicholas J. Ekins-Daukes. "Fundamental losses in solar cells". In: *Progress in Photovoltaics: Research and Applications* 19.3 (2011), pp. 286–293. DOI: https://doi.org/10.1002/pip.1024. eprint: https://onlinelibrary.wiley.com/doi/pdf/10.1002/pip.1024. URL: https://onlinelibrary.wiley.com/doi/abs/10.1002/pip.1024.

[8] Hugh D. Young and Roger A. Freedman. *University Physics with Modern Physics*. Vol. 1. Pearson, 2016. ISBN: 9781292100319.

[9] Ludovico Tesser, Robert S. Whitney, and Janine Splettstoesser. "Thermodynamic Performance of Hot-Carrier Solar Cells: A Quantum Transport Model". In: *Physical Review Applied* 19.4 (Apr. 2023). DOI: 10.1103/physrevapplied.19.044038. URL: https://doi.org/10.1103%5C%2Fphysrevapplied.19.044038.

[10] Jean-Christophe Pain. "Relations for the difference of two dilogarithms." In: (2023). URL: https://ludwig.lub.lu.se/login?url=https://search.ebscohost.com/login.aspx?direct=true&AuthType=ip,uid&db=edsarx&AN=edsarx.2304.03349&site=eds-live&scope=site.

[11] Abdelhamid Bouzaher, Amel Terki, and Mohamed Tahar Bouzaher. "Photovoltaic Panel Faults Diagnosis: Based on the Fill Factor Analysis and Use of Artificial Intelligence Techniques." In: *Arabian Journal for Science and Engineering* (2022), pp. 1–17. ISSN: 2193-567X. URL: https://ludwig.lub.lu.se/login?url=https://search.ebscohost.com/login.aspx?direct=true&AuthType=ip,uid&db=edssjs&AN=edssjs.39058B1A&site=eds-live&scope=site.

[12] Paul Horowitz and Winfield Hill. *The art of electronics.* Cambridge U.P., 1980. ISBN: 0521231515. URL: https://ludwig.lub.lu.se/login?url=https://search.ebscohost.com/login.aspx?direct=true&AuthType=ip,uid&db=cat07147a&AN=lub.1534483&site=eds-live&scope=site.

[13] Qi Boyuan and Wang Jizheng. "Fill factor in organic solar cells." In: *Physical Chemistry Chemical Physics* 15.23 (2013), pp. 8972–8982. URL: https://ludwig.lub.lu.se/login?url=https://search.ebscohost.com/login.aspx?direct=true&AuthType=ip,uid&db=inh&AN=14120921&site=eds-live&scope=site.

Appendix

Dimensionless substitutions derivation

Firstly, due to the fact that $\mu_S = 0$, all factors with μ_S will be set to 0. Now we will rewrite some of the constants/expressions to use the substitutions defined in equations (16), (17) and (18). Firstly note β_S can be rewritten as:

$$\beta_S = \frac{1}{k_B(T_{ec} + \Delta T)} = \frac{1}{k_B T_{ec}} \cdot \frac{1}{1 + \frac{\Delta T}{T_{ec}}} = \beta_{ec} \cdot \frac{1}{1 + \frac{\Delta T}{T_{ec}}} = \beta_{ec}\gamma_s \tag{23}$$

As a next step $\beta_S(U_e - \mu_s)$ can be rewritten as:

$$\beta_S(U_e - \mu_S) = \underbrace{\beta_{ec}U_e}_{\epsilon}\,\gamma_S - \underbrace{\beta_{ec}\gamma_S\mu_s}_{0} = \epsilon\gamma_S \tag{24}$$

And finally $\beta_{ec} \cdot (U_e - \mu_{ec})$ can be expressed as:

$$\beta_{ec} \cdot (U_e - \mu_{ec}) = \underbrace{\beta_{ec}U_e}_{\epsilon} - \underbrace{\beta_{ec}\mu_{ec}}_{\chi} = \epsilon - \chi \tag{25}$$

Inserting these expressions into equations (9) and (11) we obtain

$$\tau_{ec}^N = \log\left(e^{\epsilon-\chi} + 1\right) - \frac{1}{\gamma_S}\log(e^{\gamma_S \cdot \epsilon} + 1) + \chi, \tag{26}$$

$$\tau_{ec}^E = \frac{1}{\gamma^2} \cdot \left(Li_2(-e^{-\gamma_S\epsilon}) + \gamma_S\epsilon\log\left(e^{-\gamma_S\epsilon} + 1\right)\right) - \left(Li_2(-e^{\chi-\epsilon}) + (\epsilon - \chi)\log\left(e^{-\epsilon\gamma_S} + 1\right)\right) \tag{27}$$

$$- \chi\left(\log\left(e^{\epsilon-\chi} + 1\right) - (\epsilon - \chi)\right)$$